MULTISCALE MECHANICS GROUP (MSM)/TS/CTW
UNIVERSITY OF TWENTE, ENSCHEDE, NETHERLANDS
JANUARY 27, 2012

VICI Report (Project No. 10828)

To: VICI and Industrial Partners of project VICI No. 10828

From: Kuniyasu Saitoh, Postdoc

Subject: Bridging the gap between particulate systems and continuum theory

I. BACKGROUND

This report describes the progress of the VICI project 10828, *Bridging the gap between particulate systems and continuum theory.* In this progress report, we focus on the dissipative particles, for example, granular materials. If the density of granular particles is very small, we can derive the hydrodynamic equations from the kinetic theory of dissipative particles, on the other hand, there are many attempts to describe the densely packed granular materials by elastic or viscoelastic theories. Even though the both limits (extremely low and high densities) are well studied by the continuum theories, the macroscopic properties of the dissipative particles are drastically changed between the both limits, i.e., around the jamming point. Therefore, we study the various features of the jamming transition of dissipative particles in order to understand the macroscopic behaviors of granular particles near the transition point by continuum theories.

II. INTRODUCTION

Jamming is one of universal features of vast ranged materials including both thermal and athermal systems, for instance, glasses, granular particles, emulsions, colloidal suspensions, foams and etc., where constituents are arrested in disordered states so as the materials gain rigidity. Such jamming transitions are governed by temperature, density and external loads, and a lot of systems can be mapped onto the unified phase diagram of jamming transition [1–3].

Jamming of athermal systems, i.e., granular particles [4–7], emulsions [8, 9] and foams [10, 11], occurs at zero temperature. In this sense, this transition is purely mechanical. Increasing the density ϕ at zero temperature, the jamming transition occurs at the critical density ϕ_c, so-called point J [1]. At this point, each constituent or particle begins to touch with each other and mean coordination number z defined as the averaged number of contacts per particle jumps to the mechanically stable value, i.e., isostatic value $z_c = 2d$, from zero in d-dimension [12], and some macroscopic variables indicate the acquisition of rigidity, for example, pressure p and shear modulus K start to increase from zero, and bulk modulus G discontinuously jumps to non-zero value [4–7]. Slightly above this threshold, the excess coordination number $\Delta z = z - z_c$, p, K and G are scaled by the powers of the distance

from the jamming point $\Delta\phi = \phi - \phi_c$ as $\Delta z \sim \Delta\phi^{1/2}$, $p \sim \Delta\phi^{\psi}$, $K \sim \Delta\phi^{\gamma}$ and $G \sim \Delta\phi^{\lambda}$, respectively, on the analogy of critical phenomena, while some of them show discontinuous changes at the critical point like the first-order phase transitions and the critical exponents ψ, γ and λ depends on the interparticle forces, which means the jamming transition is entirely different from usual critical phenomena [4–7].

One can also find some structural signatures of jamming in monodisperse repulsive particles, where the first peak of the radial distribution function g_1 diverges as $g_1 \sim \Delta\phi^{-1}$ and its left-hand width s, which is related to the mean overlap between particles $\langle\delta\rangle$, decreases to zero as approaching to the point J from $\phi > \phi_c$ [5, 13–16]. Because $g_1 s$ or $g_1\langle\delta\rangle$ are approximately equal to the averaged number of contacts, $g_1 s \approx z_c$ or $g_1\langle\delta\rangle \approx z_c$ at just above the point J, thus both s and $\langle\delta\rangle$ are scaled as $s, \langle\delta\rangle \sim \Delta\phi$ [4–7]. The radial distribution function $g(r)$ itself also diverges as $g(r) \sim 1/\sqrt{r-1}$ $(r > 1)$ slightly above ϕ_c, where r is scaled by the particle diameter, therefore a large number of particles are on the verge of touching with each other near the jamming point. In the case of bidisperse particles, one can see a similar divergence of the function $g(\xi)$, where $\xi = r/(r_i + r_j)$ is the scaled interparticle distance and $r_i + r_j$ is the sum of radii of particles [7].

Vibrational modes of jammed particles also give us insight into the anomalous behaviors of the jamming transition, where the density of normal modes $D(\omega)$ calculated by the dynamical matrix shows an untrivial plateau in low frequencies and drops to zero at the crossover frequency ω^*, which is unexpected from the Debye model $D(\omega) \sim \omega^{d-1}$. The width of plateau and ω^* becomes larger and smaller, respectively, as the system approaches to ϕ_c from $\phi > \phi_c$, and ω^* is scaled as $\omega^* \sim \Delta z$ [17–20].

In experiments, long range correlation of forces were not found in isotropically compressed particles near the jamming point [21], therefore, the jamming transition lacked a diverging length scale despite some quantities show critical behaviors. However, the crossover frequency ω^* predicts the existence of the diverging length scale $l^* \sim \Delta z^{-1}$ [17–20], which is tested by both global and point responses of jammed particles [22–24]. Even though the localization of the chracteristic length should be discussed [25], l^* is physically important, because a coarse graining of densely packed particles [26–29] is only effective in the length scale $l > l^*$ [22–24], which means we cannot use the coarse graining method near the jamming point because of $l^* \to \infty$.

Probability distribution function (PDF) of forces also shows a sturactural signature of

jamming [30, 31]. Particles in the jammed media are supported with each other and one can see inhomogeneous distributions of forces on the force chain networks. The PDF of forces $P(f)$ above the jamming point shows a peak in the relatively small range of forces, broadening tail in the large forces, and the non-zero value at zero force $P(0) > 0$ [32–36]. From many observations of $P(f)$ in experiments and numerical simulations, $P(f)$ is well fitted by the combination of power, exponential and gaussian functions $P(f) = (C_0 + C_1 f^a)e^{-bf-cf^2}$ with the parameters C_0, C_1, a, b and c [37–42]. Because the jammed media of athermal particles does not have temperature T, usual statistical mechanics cannot be used to explain such features of $P(f)$. Therefore, based on the concept of compactivity of the static state of athermal particles [43–48], which is the analogue of the entropy, various ensemble theories [49–57], the mean field or field theories [58–62] and entropy maximizations [63–68] produced many predictions of the functional forms of $P(f)$. There is also another approach to understanding jamming of athermal systems where the theory of glass transition with finite temperature is applied to the limit of $T \to 0$ [69, 70]. Under external shear load, the jammed media is stable until the load exceeds the yield limit [71, 72] and anisotropies in $P(f)$ develops along the sheared direction [21, 73]. Below the jamming, on the other hand, one can also see the divergence of shear viscosity [74].

In this progress report, we study the static and dynamic properties of jamming transition of two-dimensional bidisperse athermal particles by numerical simulations. Many previous works of bidisperse systems focused on the case that the ratio of two different diameters equals $\rho = 1.4$ and so on. Even though the critical scalings above jamming transition are well established, the critical amplitudes have not been paid so much attention. Thus, one of our purposes is systematic studies of the size ratio and the critical amplitudes. We explain our simulation details in Sec. III. We study the static properties of jamming transition and the PDF of forces in Sec. IV. We conclude our progress in Sec. V and discuss our future works in Sec. VI.

III. DISCRETE ELEMENT METHOD (DEM)

We use the discrete element method (DEM) to demonstrate two-dimensional bidisperse dissipative particles. In Sec. III A, we introduce the model of dissipative particles and in Sec. III B, we explain our method to jam the system with the particles. In Sec. III C, we

explain a criterion of the small time step for numerical integration of the equation of motion.

A. Equation of motion

We adopt the linear viscoelastic model for interaction between two particles and do not take into account rotation of each particle. The equation of motion of i-th particle interacting with j-th particles is given by

$$m_i(t)\ddot{\mathbf{x}}_i = \sum_j \left\{k_n\delta_{ij} - \eta_n(\mathbf{v}_{ij}\cdot\mathbf{n}_{ij})\right\}\mathbf{n}_{ij} \ , \tag{1}$$

where $m_i(t)$, $\mathbf{x}_i$, k_n and η_n are the mass of the i-th particle at time t, the position of the i-th particle, the spring constant and the viscosity coefficient, respectively, and the dot represents the time derivative. The overlap δ_{ij}, the normal vector $\mathbf{n}_{ij}$ and the relative velocity $\mathbf{v}_{ij}$ are given by $\delta_{ij} = r_i(t)+r_j(t)-|\mathbf{x}_i-\mathbf{x}_j|$, $\mathbf{n}_{ij} = (\mathbf{x}_i-\mathbf{x}_j)/|\mathbf{x}_i-\mathbf{x}_j|$ and $\mathbf{v}_{ij} = \dot{\mathbf{x}}_i-\dot{\mathbf{x}}_j$, respectively, where $r_i(t)$ and $r_j(t)$ are the radii of i-th and j-th particles at time t, respectively.

B. Radius growth

We prepare 50 : 50 mixtures of the particles with different diameters $\sigma_{\rm S}(0) < \sigma_{\rm L}(0)$ and randomly distribute the particles in a $L\times L$ square periodic box, where the initial area fraction $\phi(0)$ is much less than the jamming point. To jam the system with particles, we adopt the Lubachevsky-Stillinger (LS) algorithm often used in the simulations of random close packing of hard spheres [75, 76], where the diameter of each particle is slowly increased [77]. The LS algorithm mimics isotropic compression, or more directly, the tunable-diameter colloids [78–85]. We increase the diameter of each particle with the constant speed

$$\dot{\sigma}_i(t) = g_r\sigma_i(0) \ , \tag{2}$$

where g_r and $\sigma_i(0)$ are the growth rate and the initial diameter, respectively, and the subscript i = L and S represents the large and small particles, respectively. Because we fix the density of mass of particle, the mass of particle $m_i(t)$ is also increased. From Eq.(2), $\sigma_i(t) = \sigma_i(0)(g_rt+1)$, thus the ratio of two different diameters

$$\rho = \frac{\sigma_{\rm L}(t)}{\sigma_{\rm S}(t)} = \frac{\sigma_{\rm L}(0)}{\sigma_{\rm S}(0)} \ , \tag{3}$$

does not change through the simulation. When the area fraction $\phi(t)$ reaches to the target value $\phi(t_0) = \phi$ at $t = t_0$, we stop to increase the diameter, thus the diameter of large particle at $t = t_0$ is given by

$$\sigma_{\rm L}(t_0) = \sqrt{\frac{8\phi}{\pi\rho_N(1+1/\rho^2)}} \ , \tag{4}$$

where ρ_N is the number density of particles.

In the following sections, we introduce the units of mass, length and time as $m_u = m_{\rm L}(t_0)$, $l_u = \sigma_{\rm L}(t_0)$ and $t_u = m_{\rm L}(t_0)/\eta_n$, respectively, and use $k_n = 1.0 \times 10^4 m_u/t_u^2$ and $g_r = 0.04$ in Eqs. (1) and (2), respectively. In Sec. IV, we prepare $N = 32768$ particles in the $L \times L$ periodic box with $L = \sqrt{\pi N/4\phi} l_u$, where the initial diameter of large and small particles are given by $0.7 l_u$ and $0.7 l_u/\rho$, respectively, which gives the initial area fraction $\phi(0) = 0.49\phi$. We change the target area fraction ϕ and the size ratio ρ in the ranges $0.8 \leq \phi \leq 0.9$ and $1.2 \leq \rho \leq 2.4$, respectively.

C. Criterion for the small time step

To integrate Eq.(1) numerically, the small time step h should be much less than the typical response time

$$t_c = \frac{\pi}{\sqrt{(k_n/m_{ij}) - \eta_0^2}} \ , \tag{5}$$

where $m_{ij} = m_i(t_0)m_j(t_0)/(m_i(t_0) + m_j(t_0))$ and $\eta_0 = \eta_n/(2m_{ij})$ are the reduced mass and the scaled viscosity coefficient, respectively [86]. In our bidisperse systems, t_c is the smallest if m_{ij} is given by two small particles and we use $h \simeq t_c \times 10^{-2}$. The restitution coefficient e is given by

$$e = \exp(-\eta_0 t_c) \ , \tag{6}$$

and we find $e \simeq 0.99$ for every combinations of particles if ϕ and ρ are in the ranges $0.8 \leq \phi \leq 0.9$ and $1.2 \leq \rho \leq 2.4$, respectively.

IV. STATIC PROPERTIES OF JAMMING TRANSITION

During the diameter $\sigma_i(t)$ grows as Eq. (2), each particle gets into contact with the surrounding particles. As a result, the particles are pushed and moved. The mass $m_i(t)$ is

also increased, thus the kinetic energy per particle $K_p(t)$ is increased at first. When $\phi(t)$ reaches to the target value ϕ, we stop to increase the diameter and $K_p(t)$ is decreased by the inelastic collisions between particles, and finally, the system relaxes to the static state $K_p(\infty) \simeq 0$. In our simulation, we assume the system is static if $K_p(t) < 10^{-10}$. If the system becomes static and ϕ is larger than the critical area fraction ϕ_c, particles are arrested in the disordered state and we observe force chain networks as shown in Fig. 1. In this figure, the red solid line connects interacting two particles, where the width is proportional to the strength of interacting forces, and the blue solid line connects the nearest neighbors without contacts so as the red and blue lines constract the edges of the Delaunay graph [87]. In the following subsections, we study the static properties of the jamming transition. In Sec. IV A, we explain our results of ϕ_c. In Sec. IV B, we show the power law scalings of the coordination number, the pressure, the mean overlap and the maximum overlap above the jamming point. In Sec. IV C, we explain the radial distribution function of the scaled distance $g(\xi)$, which is more suitable for bidisperse systems than the usual difinition of the radial distribution function, and show the divergence of the first peak of $g(\xi)$. In Sec. IV D, we explain our results of the PDF of forces.

A. Critical area fraction

We define the critical area fraction ϕ_c as the point at which the coordination number z jumps to the isostatic value $z_c = 4$ from zero. Above the jamming point, we remove *rattlers* of which the number of contacts are less than 3 from our systems, because they do not have any contribution to the force chain networks. The critical area fraction slightly increases from $\rho = 1.2$ to 2.4 as shown in Fig. 2, where the open circles represent our simulation results. Such a dependence of ϕ_c on ρ can be explained if we consider an isostatic configuration as shown in Fig. 3, where $r_{\rm L}$ and $r_{\rm S} = r_{\rm L}/\rho$ are the radii of large and small particles, respectively. The area fraction in the solid square is given by

$$\phi_1 = \frac{\pi}{2}\frac{\rho^2+1}{(\rho+1)^2} , \tag{7}$$

if $r_{\rm L}$ is less than the edge of the solid square, i.e., $r_{\rm L} \le (r_{\rm L} + r_{\rm S})/\sqrt{2}$ which is equivalent to $(1 + 1/\rho) \ge \sqrt{2}$ and always satisfied if $1.2 \le \rho \le 2.4$. If the large and small particles are regularly arranged as Fig. 3, the system is tiled with the solid square in Fig. 3. On the

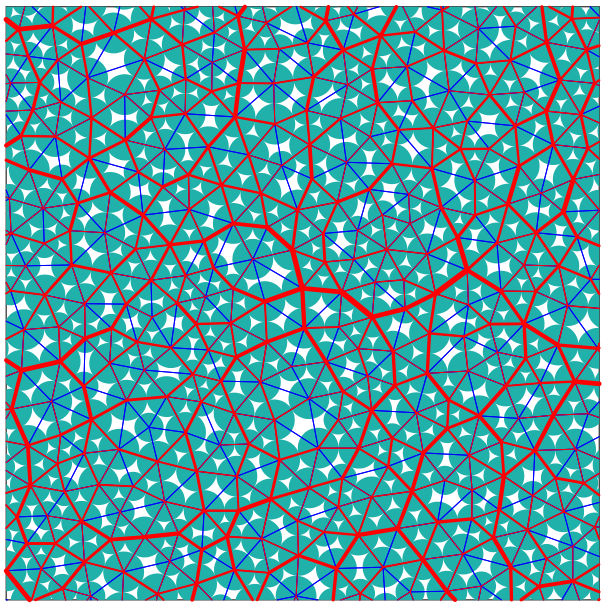

FIG. 1. Force chain network above the jamming point. The red and blue solid lines respectively represent the *real* and *virtual* contacts, where the width of the red solid line is proportional to the strength of force between interacting two particles and the blue solid line connects the nearest neighbors without contacts. The red and blue lines constract the edges of the Delaunay graph.

other hand, the area fraction of square occupied by the same kind of particles is given by $\phi_2 = \pi/4$. Then, ϕ_c is given by the weighted sum

$$\phi_c = w_1\phi_1 + w_2\phi_2 \ , \tag{8}$$

where w_1 and w_2 are the weights of ϕ_1 and ϕ_2, respectively. The solid line in Fig. 2 is Eq.(8) with $w_1 = 0.1213$ and $w_2 = 0.9550$ ($w_1 + w_2 \simeq 1$). Although the isostatic configurations in our simulations are much more complicated than Fig. 3, the numerical result of ϕ_c is well explained by our simple model. It should be noticed, however, ϕ_c is influenced by the system size and the procedures for jamming, for instance, the growth rate and the initial condition, etc [4, 5, 88, 89].

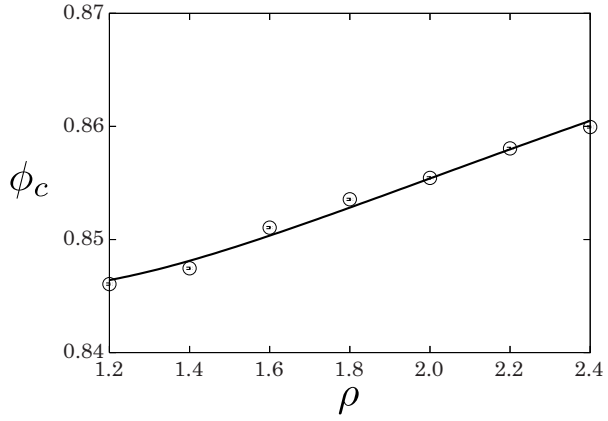

FIG. 2. Critical area fraction ϕ_c as a function of ρ, where the open circles and the solid line is our simulation results and Eq. (8), respectively.

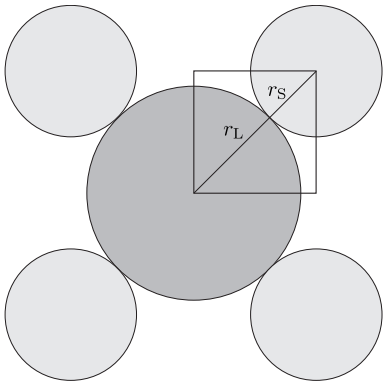

FIG. 3. An isostatic configuration of a large particle and four small particles, where $r_{\rm L}$ and $r_{\rm S}$ are the radii of the large and small particles, respectively, and the edge length of the solid square is given by $(r_{\rm L} + r_{\rm S})/\sqrt{2}$.

B. Power law scalings of jamming

Slightly above the jamming point, $\langle\delta\rangle$, Δz and p are scaled as

$$\langle\delta\rangle = A_\delta(\rho)\Delta\phi^\mu \ , \tag{9}$$

$$\Delta z = A_z(\rho)\Delta\phi^\zeta \ , \tag{10}$$

$$p = A_p(\rho)\Delta\phi^\psi \ , \tag{11}$$

respectively [4–7], where the pressure is defined as $p = \sum_{i<j} r_{ij} f_{ij}/(2L^2)$ with the interparticle distance r_{ij} and force f_{ij} [90]. In Eqs. (9)-(11), the *critical exponents* μ, ζ and ψ do not depend on ρ, however, the *critical amplitudes* $A_\delta(\rho)$, $A_z(\rho)$ and $A_p(\rho)$ are the functions

of ρ. From our simulation, we also find that the maximum overlap $\delta_{\rm m}$ is scaled as

$$\delta_{\rm m} = A_{\rm m}(\rho)\Delta\phi^{\lambda} \ . \tag{12}$$

Figure 4 displays normalized variables $\langle\delta\rangle^* \equiv \langle\delta\rangle/A_\delta(\rho)$, $\Delta z^* \equiv \Delta z/A_z(\rho)$, $p^* \equiv p/A_p(\rho)$ and $\delta^*_{\rm m} \equiv \delta_{\rm m}/A_{\rm m}(\rho)$, where $1.2 \leq \rho \leq 2.2$ and the best fit scalings give $\mu = 1.0 \pm 0.003$, $\zeta = 0.55 \pm 0.001$, $\psi = 1.03 \pm 0.0006$ and $\lambda = 0.97 \pm 0.001$, respectively. Therefore we confirm $\Delta z \sim \Delta\phi^{1/2}$ and $\langle\delta\rangle, p \sim \Delta\phi$, and find $\delta_{\rm m} \sim \Delta\phi$. In Fig. 5, we also plot the critical amplitudes, where $A_\delta(\rho)$, $A_z(\rho)$, $A_p(\rho)$ and $A_{\rm m}(\rho)$ becomes smallest around $\rho = 1.8$.

The overlap δ is defined between interacting two particles, i.e., defined on the *real* contact (the red solid line in Fig. 1), therefore, the mean overlap $\langle\delta\rangle$ is meaningful only if $\phi > \phi_c$ because $\langle\delta\rangle = 0$ in $\phi < \phi_c$. However, each particle can be also connected with the nearest neighbors without contact by the *virtual* contact (the blue solid line in Fig. 1), and we can also define $\delta = r_i + r_j - |\mathbf{x}_i - \mathbf{x}_j|$ on these lines. Such "overlaps" are negative and the mean value extended to the negative region $\langle\delta\rangle_{\rm G} \equiv \langle\delta\rangle + \langle\delta\rangle_-$, where $\langle\delta\rangle_-$ is the mean value of negative overlaps, is also defined in $\phi < \phi_c$. Figure 6 is $\langle\delta\rangle_{\rm G}$ as a function of ϕ, where the vertical dotted line is the border between below and above ϕ_c. To calculate $\langle\delta\rangle_{\rm G}$ below the jamming point, we do not remove rattlers from our systems. From this figure, we find a discontinuous change of $\langle\delta\rangle_{\rm G}$ at ϕ_c. Therefore, $\langle\delta\rangle_{\rm G}$ is one of the signatures of jamming transition below ϕ_c. Far below ϕ_c, $\langle\delta\rangle_{\rm G}$ increases linearly with the slope 0.357. Far above ϕ_c, $\langle\delta\rangle_{\rm G}$ asymptotically approaches to the same line. However, it should be noted that both $\langle\delta\rangle_{\rm G}$ and $\langle\delta\rangle_-$ cannot be scaled by the power of $|\Delta\phi|$.

C. Radial distribution function

In monodisperse systems, the first peak of the radial distribution function $g(r)$ diverges as $\Delta\phi^{-1}$ above the jamming point, which is one of the structural signatures above jamming [4–7]. In bidisperse systems, however, the radial distribution function $g(r)$ has three peaks around $\sigma_{\rm S}$, $\sigma_{\rm L}$ and $(\sigma_{\rm L} + \sigma_{\rm S})/2$, respectively, thus we need to introduce more appropriate expression for the structure of bidisperse systems. If we scale the distance between i-th and j-th particles r as

$$\xi = \frac{r}{r_i + r_j} \ , \tag{13}$$

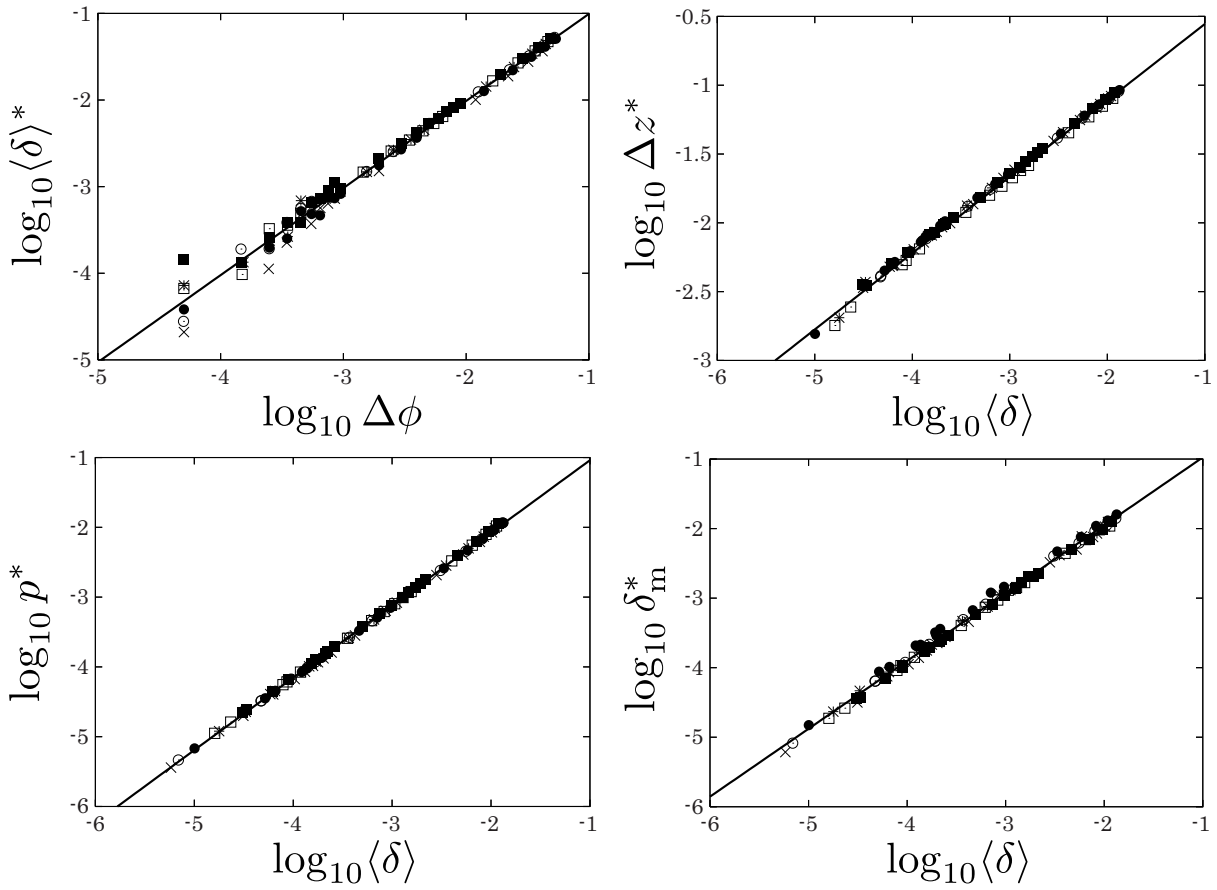

FIG. 4. Double logarithm plots of $\langle\delta\rangle^*$ (upper-left panel), z^* (upper-right panel), p^* (lower-left panel), $\delta^*_{\rm m}$ (lower-right panel), respectively, where z^*, p^* and $\delta^*_{\rm m}$ are plotted as functions of $\langle\delta\rangle$. The filled circles, open circles, filled squares, open squares, stars and crosses are the results of $\rho = 1.2$, 1.4, 1.6, 1.8, 2.0 and 2.2, respectively.

where r_i and r_j are the radii of i-th and j-th particles, respectively, a similar divergence of the function $g(\xi)$ can be seen [7], however, the results are not shown in Ref. [7]. Figure 7 shows our results of $g(\xi)$, where we scaled the system size L by the mean value of $r_i + r_j$, i.e., $(3/2 + 1/\rho)l_u$, and the first peak is found around $\xi = 1$. As shown in Fig. 8, we can see discontinuous jumps at $\xi = 1$ in both below and above ϕ_c. Such discontinuous jumps of the radial distribution functions are also found in the "jamming" as the zero temperature limit of monodisperse glass transitions [70]. Slightly above the jamming point, the first peak of $g(\xi)$ diverges as

$$g_+ = A_+(\rho)\Delta\phi^{-\eta_+} \ . \tag{14}$$

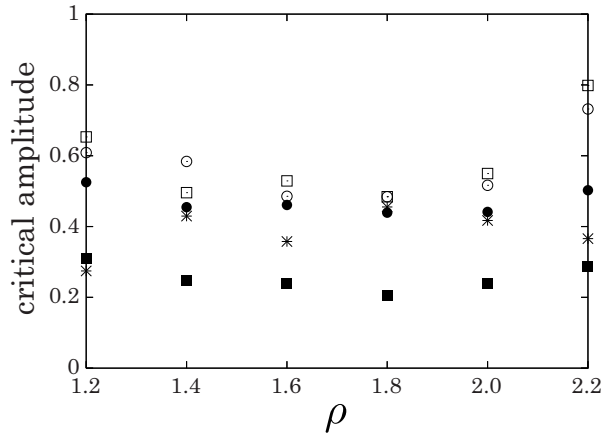

FIG. 5. Critical amplitudes as functions of ρ, where The filled circles, open circles, filled squares, open squares and stars are $A_z(\rho)\times 10^{-1}$, $A_p(\rho)\times 10^{-4}$, $A_\delta(\rho)$, $A_{\rm m}(\rho)\times 0.5$ and $A_+(\rho)$, respectively.

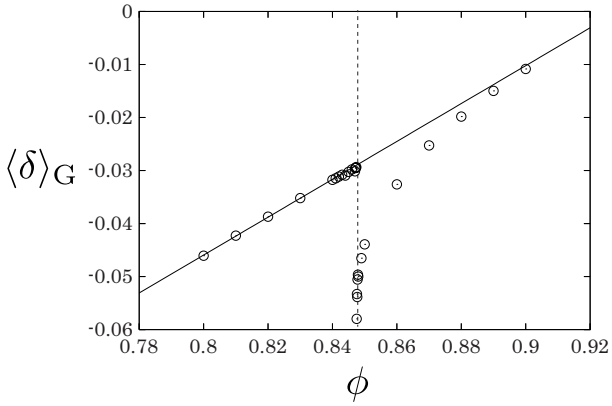

FIG. 6. Extended mean overlap $\langle\delta\rangle_{\rm G}$ as a function of ϕ, where $\rho = 1.4$. The vertical dotted line is the border between below and above ϕ_c.

We plot $A_+(\rho)$ and $g_+^* \equiv g_+/A_+(\rho)$ in Figs. 5 and 9, respectively, where we find $\eta_+ = 0.962 \pm 0.001$. Therefore, from Eqs. (9) and (14), we reconfirm the important relation $g_+\langle\delta\rangle \approx$ const.

D. Probability distribution function of forces

The PDF of forces $P(f)$ also indicates a signature of jamming [30, 31]. Figure 10 (left) is our results of the PDFs of forces with $\rho = 1.4$ and different ϕ. Slightly above the jamming point, $P(f)$ has sharp peak near $f = 0$. The sharp peak is leveled and $P(f)$ is broadened as

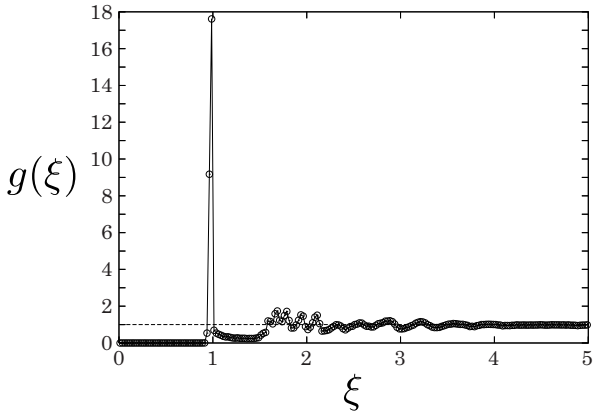

FIG. 7. The radial distribution function of the scaled distance $g(\xi)$, where $\rho = 1.4$ and $\Delta\phi = 5.25 \times 10^{-2}$.

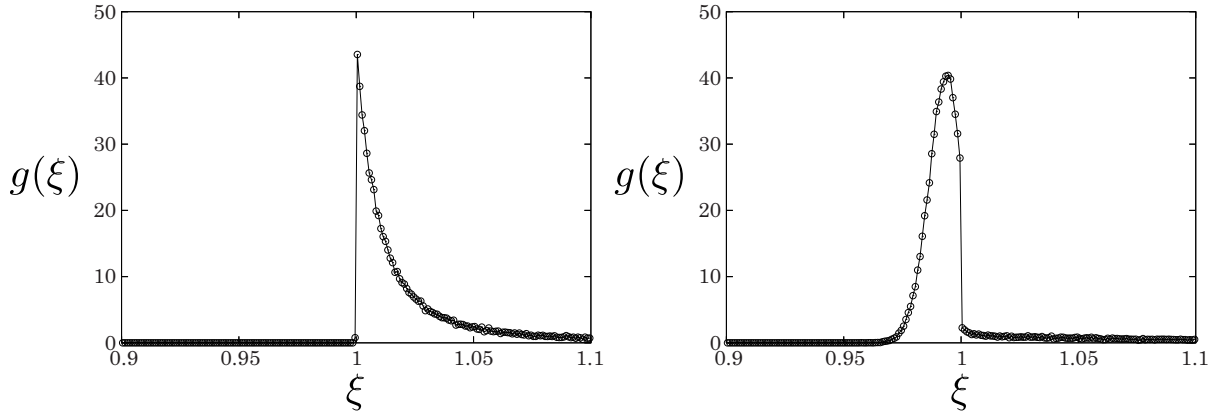

FIG. 8. Discontinuous jumps of $g(\xi)$ at $\xi = 1$, where $\rho = 1.4$, and $\Delta\phi = -1.74 \times 10^{-2}$ (left) and $\Delta\phi = 2.25 \times 10^{-2}$ (right), respectively.

ϕ goes away from ϕ_c. Figure 10 (right) is the scaled PDF of forces $P(f^*)$, where the force is normalized by the mean value as $f^* \equiv f/\langle f \rangle$. In this figure, the PDFs of forces with different ϕ are collapsed. We find such collapse can be seen in $\Delta\phi < 10^{-1}$, however, the PDFs of forces in $\Delta\phi > 10^{-1}$ decays much faster and cannot be collapsed. The solid curve in Fig. 10 (right) is the empirical fitting function

$$P(f^*) = (A_0 + A_1 f^{*a_0}) e^{-a_1 f^* - a_2 f^{*2}} , \tag{15}$$

where the fitting parameters are given by $A_0 = 0.076$, $A_1 = 0.74$, $a_0 = 0.23$, $a_1 = 0.11$ and $a_2 = 0.36$, respectively. Figure 11 (left) is the logarithm plot of $P(f^*)$ as a function of f^*, where $P(f^*)$ in $f^* < 1$ can be well fitted by the solid line $f^{*a_0} e^{-a_1 f^*}$ predicted by the

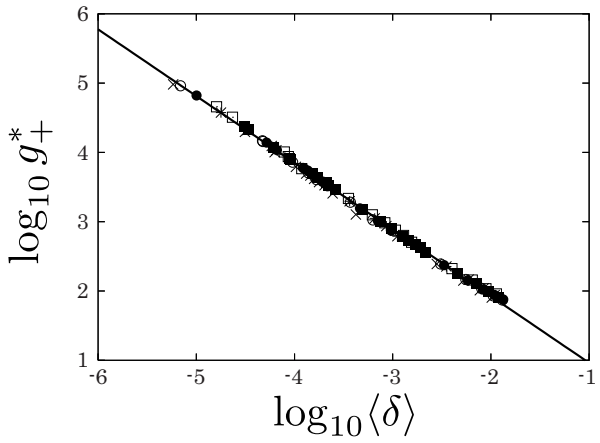

FIG. 9. Double logarithm plot of g_+^* as a function of $\langle\delta\rangle$. The filled circles, open circles, filled squares, open squares, stars and crosses are the results of $\rho = 1.2$, 1.4, 1.6, 1.8, 2.0 and 2.2, respectively.

so-called q-model, however, $P(f^*)$ decays much faster than $f^{*a_0}e^{-a_1 f^*}$ above $f^* = 1$. Figure 11 (right) is the logarithm plot of $P(f^*)$ as a function of f^{*2}, where the solid line represents the Gaussian function $e^{-a_2 f^{*2}}$. Such a Gaussian decay in large forces is also pointed out in the study of umbrella sampling of force network ensembles [42], where it can be seen in extremely large forces $f^* > 5$ that $P(f^*)$ decays faster as approacing the jamming point. In our DEM simulation, however, $P(f^*)$ cannot reach the regime $f^* > 5$ and significant difference of $P(f^*)$ cannot be seen. In Fig. 12, we display the fitting parameters A_0, A_1, a_0, a_1 and a_2 as functions of ρ.

Becuase we use Eq. (1) and the system is in static state, the forces is directly connected to the overlaps as $f = k_n\delta$ and $\langle f\rangle = k_n\langle\delta\rangle$. If $P(f)$ is also given by [37–42]

$$P(f) = (B_0 + B_1 f^{b_0})e^{-b_1 f - b_2 f^2} \ , \tag{16}$$

Eqs. (9) and (16), and the relation $P(f^*) = \langle f\rangle P(f)$ lead the following scalings

$$B_0 \propto \Delta\phi^{-1} \ , \tag{17}$$

$$B_1 \propto \Delta\phi^{-(a_0+1)} \ , \tag{18}$$

$$b_0 = a_0 \ , \tag{19}$$

$$b_1 \propto \Delta\phi^{-1} \ , \tag{20}$$

$$b_2 \propto \Delta\phi^{-2} \ . \tag{21}$$

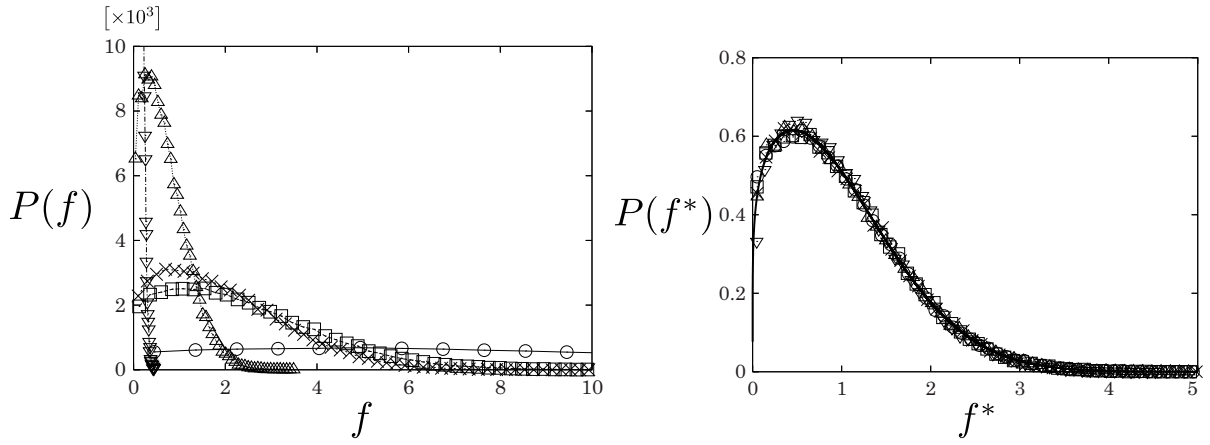

FIG. 10. The PDFs of forces $P(f)$ (left) and $P(f^*)$ (right), where $\rho = 1.4$ and the solid line in the right panel is Eq. (15). Here, the open circles, open squares, crosses, open triangles and open inverted-triangles are the results of $\Delta\phi = 1.3 \times 10^{-2}$, $\Delta\phi = 5.5 \times 10^{-4}$, $\Delta\phi = 4.5 \times 10^{-4}$, $\Delta\phi = 2.5 \times 10^{-4}$ and $\Delta\phi = 5.0 \times 10^{-5}$, respectively.

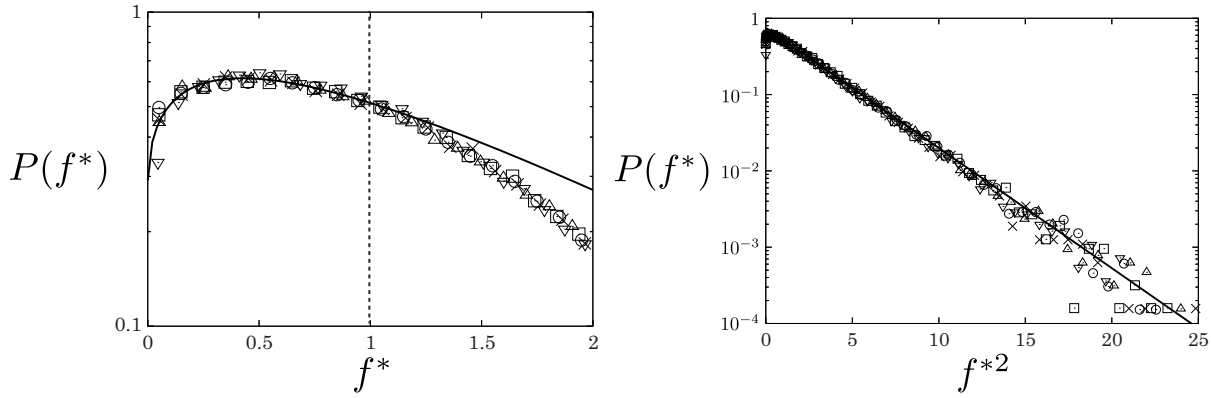

FIG. 11. The logarithm plots of $P(f^*)$ as functions of f^* (left) and f^{*2} (right) where $\rho = 1.4$. The solid lines in the left and right panels are $f^{*a_0}e^{-a_1 f^*}$ and $e^{-a_2 f^{*2}}$, respectively. Here, the open circles, open squares, crosses, open triangles and open inverted-triangles are the results of $\Delta\phi = 1.3 \times 10^{-2}$, $\Delta\phi = 5.5 \times 10^{-4}$, $\Delta\phi = 4.5 \times 10^{-4}$, $\Delta\phi = 2.5 \times 10^{-4}$ and $\Delta\phi = 5.0 \times 10^{-5}$, respectively.

Because of $P(f) = P(k_n\delta)$, the function $g(1-\xi)$ $(\xi < 1)$ is equivalent to $P(f)$ and $P(0) = B_0$ is diverges in the same way with the first peak g_+, which is consistent with Eq. (17). We also confirmed Eq. (20) is correct in our simulation and other scalings indicate that $P(f)$ shows the structural signature of jamming transition as shown in Fig. 10 (left).

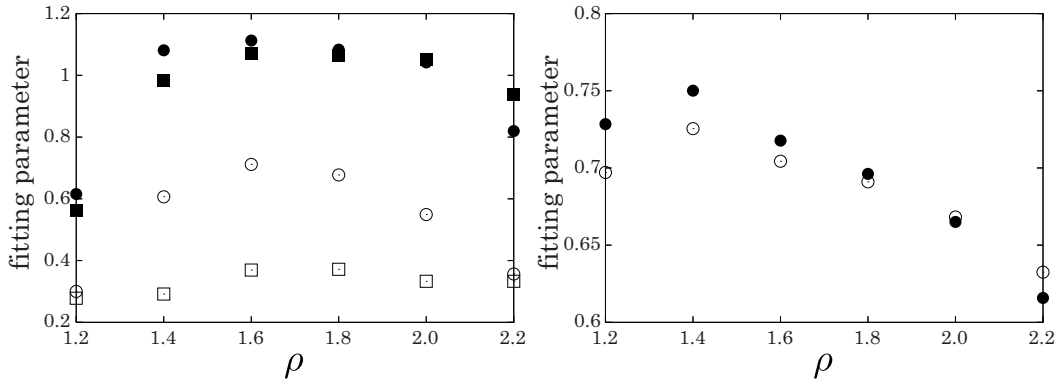

FIG. 12. Fitting parameters A_0, A_1, a_0, a_1 (left) and a_2 (right) as functions of ρ. In the left panel, the open squares, filled circles, open circles and filled squares are the results of A_0, A_1, a_0 and a_1. In the right panel, the filled circles are the results of a_2. .

V. SUMMARY

In summary, we numerically investigated the static properties of jamming transition of two dimensional bidisperse dissipative particles. Especially, we systematically studied the influence of size ratio ρ and show results of the critical amplitudes which were not paid so much attention in the previous works. We also found the new scaling law of the maximum overlap $\delta_{\rm m} \propto \Delta\phi$ and introduced the extended mean overlap $\langle\delta\rangle_{\rm G}$ which indicate the signature of jamming transition below the jamming point. We also showed the results of the radial distribution function of scaled distance $g(\xi)$, which is more suitable for the structures of bidisperse systems than the usual definition of $g(r)$, and found the divergence of the first peak of $g(\xi)$. In our studies of the PDF of forces, we found the collapse of $P(f)$ of different density and proposed some ciritcal scalings of the coefficients in the fitting function of $P(f)$.

VI. FUTURE WORKS

We studied the bidisperse systems with the size ratio in $1.2 \leq \rho \leq 2.4$ to avoid cristallization of particles. Thus, the study of monodisperse and polydisperse cases are our future works. In addition, the studies in 3-dimension are also our future works. Although we discussed the influence of system size, we did not discuss the influences of the growth rate g_r and the restitution coefficient e. Therefore, we will study the dependence on g_r and e in

our future works.

---

[1] A. J. Liu and S. R. Nagel, Nature (London) **396**, 21 (1998).

[2] V. Trappe, V. Prasad, L. Cipelletti, P. N. Segre, and D. A. Weitz, Nature **411**, 772 (2001).

[3] C. Song, P. Wang, and H. A. Makse, Nature **453**, 629 (2008).

[4] C. S. O'Hern, S. A. Langer, A. J. Liu, and S. R. Nagel, Phys. Rev. Lett. **88**, 075507 (2002).

[5] C. S. O'Hern, L. E. Silbert, A. J. Liu, and S. R. Nagel, Phys. Rev. E **68**, 011306 (2003).

[6] T. S. Majmudar, M. Sperl, S. Luding, and R. P. Behringer, Phys. Rev. Lett. **98**, 058001 (2007).

[7] M. van Hecke, J. Phys.: Condens. Matter **22**, 033101 (2010).

[8] J. Brujić, S. F. Edwards, D. V. Grinev, I. Hopkinson, D. Brujić, and H. A. Makse, Faraday Discuss. **123**, 207 (2003).

[9] H. P. Zhang and H. A. Makse, Phys. Rev. E **72**, 011301 (2005).

[10] F. Bolton and D. Weaire, Phys. Rev. Lett. **65**, 3449 (1990).

[11] D. J. Durian, Phys. Rev. Lett. **75**, 4780 (1995).

[12] S. Alexander, Phys. Rep. **296**, 65 (1998).

[13] L. E. Silbert, D. Ertaş, G. S. Grest, T. C. Halsey, and D. Levine, Phys. Rev. E **65**, 031304 (2002).

[14] L. E. Silbert, A. J. Liu, and S. R. Nagel, Phys. Rev. E **73**, 041304 (2006).

[15] A. Donev, S. Torquato, and F. H. Stillinger, Phys. Rev. E **71**, 011105 (2005).

[16] X. Cheng, Phys. Rev. E **81**, 031301 (2010).

[17] L. E. Silbert, A. J. Liu, and S. R. Nagel, Phys. Rev. Lett. **95**, 098301 (2005).

[18] M. Wyart, L. E. Silbert, S. R. Nagel, and T. A. Witten, Phys. Rev. E **72**, 051306 (2005).

[19] M. Wyart, S. R. Nagel, and T. A. Witten, Europhys. Lett. **72(3)**, 486 (2005).

[20] L. E. Silbert, A. J. Liu, and S. R. Nagel, Phys. Rev. E **79**, 021308 (2009).

[21] T. S. Majmudar and R. P. Behringer, Nature **435**, 1079 (2005).

[22] W. G. Ellenbroek, E. Somfai, M. van Hecke, and W. van Saarloos, Phys. Rev. Lett. **97**, 258001 (2006).

[23] W. G. Ellenbroek, M. van Hecke, and W. van Saarloos, Phys. Rev. E **80**, 061307 (2009).

[24] W. G. Ellenbroek, Z. Zeravcic, W. van Saarloos, and M. van Hecke, Europhys. Lett. **87**, 34004 (2009).

[25] Z. Zeravcic, W. van Saarloos, and D. R. Nelson, Europhys. Lett. **83**, 44001 (2008).

[26] I. Goldhirsch and C. Goldenberg, Eur. Phys. J. E **9**, 245 (2002).

[27] C. Goldenberg and I. Goldhirsch, Phys. Rev. Lett. **89**, 084302 (2002).

[28] C. Goldenberg and I. Goldhirsch, Nature (London) **435**, 188 (2005).

[29] C. Goldenberg, A. P. F. Atman, P. Claudin, G. Combe, and I. Goldhirsch, Phys. Rev. Lett. **96**, 168001 (2006).

[30] C. S. O'Hern, S. A. Langer, A. J. Liu, and S. R. Nagel, Phys. Rev. Lett. **86**, 111 (2001).

[31] E. I. Corwin, H. M. Jaeger, and S. R. Nagel, Nature **435**, 1075 (2005).

[32] F. Radjai, M. Jean, J.-J. Moreau, and S. Roux, Phys. Rev. Lett. **77**, 274 (1996).

[33] S. Luding, Phys. Rev. E **55**, 4720 (1997).

[34] F. Radjai, S. Roux, and J.-J. Moreau, Chaos **9**, 544 (1999).

[35] L. E. Silbert, G. S. Grest, and J. W. Landry, Phys. Rev. E **66**, 061303 (2002).

[36] J. W. Landry, G. S. Grest, L. E. Silbert, and S. J. Plimpton, Phys. Rev. E **67**, 041303 (2003).

[37] D. M. Mueth, H. M. Jaeger, and S. R. Nagel, Phys. Rev. E **57**, 3164 (1998).

[38] S. J. Antony, Phys. Rev. E **63**, 011302 (2000).

[39] D. L. Blair, N. W. Mueggenburg, A. H. Marshall, H. M. Jaeger, and S. R. Nagel, Phys. Rev. E **63**, 041304 (2001).

[40] J. M. Erikson, N. W. Mueggenburg, H. M. Jaeger, and S. R. Nagel, Phys. Rev. E **66**, 040301(R) (2002).

[41] M.-K. Müller, S. Luding, and T. Pöschel, Chem. Phys. **375**, 600 (2010).

[42] A. R. T. van Eerd, W. G. Ellenbroek, M. van Hecke, J. H. Snoeijer, and T. J. H. Vlugt, Phys. Rev. E **75**, 060302(R) (2007).

[43] S. F. Edwards and R. B. S. Oakeshott, Physica A **157**, 1080 (1989).

[44] S. F. Edwards and R. B. S. Oakeshott, Physica D **38**, 88 (1989).

[45] S. F. Edwards and D. V. Grinev, Phys. Rev. Lett. **82**, 5397 (1999).

[46] S. F. Edwards and D. V. Grinev, Chaos **9**, 551 (1999).

[47] R. Blumenfeld and S. F. Edwards, Phys. Rev. Lett. **90**, 114303 (2003).

[48] R. K. Bowles and S. S. Ashwin, Phys. Rev. E **83**, 031302 (2011).

[49] C. h. Liu, S. R. Nagel, D. A. Schecter, S. N. Coppersmith, S. Majumdar, O. Narayan, and T. A. Witten, Science **269**, 513 (1995).

[50] S. N. Coppersmith, C. h. Liu, S. Majumdar, O. Narayan, and T. A. Witten, Phys. Rev. E **53**, 4673 (1996).

[51] J. H. Snoeijer, M. van Hecke, E. Somfai, and W. van Saarloos, Phys. Rev. E **67**, 030302(R) (2003).

[52] J. H. Snoeijer, M. van Hecke, E. Somfai, and W. van Saarloos, Phys. Rev. E **70**, 011301 (2004).

[53] J. H. Snoeijer, T. J. H. Vlugt, M. van Hecke, and W. van Saarloos, Phys. Rev. Lett. **92**, 054302 (2004).

[54] J. H. Snoeijer, T. J. H. Vlugt, W. G. Ellenbroek, M. van Hecke, and J. M. J. van Leeuwen, Phys. Rev. E **70**, 061306 (2004).

[55] B. P. Tighe, J. E. S. Socolar, D. G. Schaeffer, W. G. Mitchener, and M. L. Huber, Phys. Rev. E **72**, 031306 (2005).

[56] B. P. Tighe, A. R. T. van Eerd, and T. J. H. Vlugt, Phys. Rev. Lett. **100**, 238001 (2008).

[57] B. P. Tighe, J. H. Snoeijer, T. J. H. Vlugt, and M. van Hecke, Soft Matter **6**, 2908 (2010).

[58] P. T. Metzger, Phys. Rev. E **70**, 051303 (2004).

[59] A. Fierro, M. Nicodemi, M. Tarzia, A. de Candia, and A. Coniglio, Phys. Rev. E **71**, 061305 (2005).

[60] S. Henkes and B. Chakraborty, Phys. Rev. Lett. **95**, 198002 (2005).

[61] S. Henkes, C. S. O'Hern, and B. Chakraborty, Phys. Rev. Lett. **99**, 038002 (2007).

[62] S. Henkes and B. Chakraborty, Phys. Rev. E **79**, 061301 (2009).

[63] N. P. Kruyt and L. Rothenburg, Int. J. Solids Struct. **39**, 571 (2002).

[64] N. P. Kruyt, Int. J. Solids Struct. **40**, 3537 (2003).

[65] K. Bagi, Granular Matter **5**, 45 (2003).

[66] S. F. Edwards and D. V. Grinev, Granular Matter **4**, 147 (2003).

[67] A. H. W. Ngan, Phys. Rev. E **68**, 011301 (2003).

[68] P. T. Metzger, Phys. Rev. E **77**, 011307 (2008).

[69] Z. Zhang, N. Xu, D. T. N. Chen, P. Yunker, A. M. Alsayed, K. B. Aptowicz, P. Habdas, A. J. Liu, S. R. Nagel, and A. G. Yodh, Nature **459**, 230 (2009).

[70] L. Berthier, H. Jacquin, and F. Zamponi, Phys. Rev. E **84**, 051103 (2011).

[71] N. Xu and C. S. O'Hern, Phys. Rev. E **73**, 061303 (2006).

[72] S. Karmakar, E. Lerner, and I. Procaccia, Phys. Rev. E **82**, 055103(R) (2010).

[73] J. H. Snoeijer, W. G. Ellenbroek, T. J. H. Vlugt, and M. van Hecke, Phys. Rev. Lett. **96**, 098001 (2006).

[74] P. Olsson and S. Teitel, Phys. Rev. Lett. **99**, 178001 (2007).

[75] G. Prisi and F. Zamponi, Rev. Mod. Phys. **82**, 789 (2010).

[76] A. Donev, S. Torquato, F. H. Stillinger, and R. Connelly, J. App. Phys. **95**, 989 (2004).

[77] B. D. Lubachevsky and F. H. Stillinger, J. Stat. Phys. **60**, 561 (1990).

[78] H. Senff and W. Richtering, J. Chem. Phys. **111**, 1750 (1999).

[79] B. R. Saunders and B. Vincent, Adv. Colloid Interf. Sci. **80**, 1 (1999).

[80] R. Pelton, Adv. Colloid Interf. Sci. **85**, 1 (2000).

[81] J. Wu, B. Zhou, and Z. Hu, Phys. Rev. Lett. **90**, 048304 (2003).

[82] L. A. Lyon, J. D. Debord, S. B. Debord, C. D. Jones, J. G. McGrath, and M. J. Serpe, J. Phys. Chem. B **108**, 19099 (2004).

[83] A. M. Alsayed, M. F. Islam, J. Zhang, P. J. Collings, and A. G. Yodh, Science **309**, 1207 (2005).

[84] Y. Han, Y. Shokef, A. M. Alsayed, P. Yunker, T. C. Lubensky, and A. G. Yodh, Nature **456**, 898 (2008).

[85] Y. Han, N. Y. Ha, A. M. Alsayed, and A. G. Yodh, Phys. Rev. E **77**, 041406 (2008).

[86] S. Luding, J. Phys.: Condens. Matter **17**, S2623 (2005).

[87] M. de Berg, M. van Kreveld, M. Overmars, and O. Schwarzkopf, *Computational Geometry* (Springer-Verlag, Berlin Heidelberg, 1997).

[88] S. Torquato, T. M. Truskett, and P. G. Debenedetti, Phys. Rev. Lett. **84**, 2064 (2000).

[89] N. Xu, J. Blawzdziewicz, and C. S. O'Hern, Phys. Rev. E **71**, 061306 (2005).

[90] M. P. Allen and D. J. Tildesley, *Computer Simulation of Liquids* (Oxford University Press, New York, 1987).